MULTISOURCE DATA FUSION

WITH AN INTEGRATED AND UNIFIED GEOMETRIC MODELLING

Thierry Toutin
Canada Centre for Remote Sensing
588 Booth Street
Ottawa, Ontario, Canada K1A 0Y7

ABSTRACT

This paper presents a method of generating precise multi-source ortho-images using a digital elevation model and a few ground control points (4-7). This method has been integrated to take into account the geometric distortions of the full viewing geometry (sensor - platform - Earth), and unified to process raw images from different sensors (visible and radar) on various platforms (airborne and spaceborne) at different resolutions. Results from eight types of images show an absolute accuracy of 1/3 of a pixel for satellite images in the visible, one resolution cell for satellite radar images and one to two resolution cells for airborne images. Furthermore, a relative registration accuracy of one pixel is achieved in the data fusion. Integration (mosaics and colour composites) of these ortho-images with the road network overlaid confirms the relative and absolute accuracies.

1. INTRODUCTION

Cartographic and thematic applications in remote sensing use and process multi-source data (multi-date images from different sensors, topographic and thematic maps, raster and vector data) to take advantage of their complementarity (visible vs radar; airborne vs spaceborne; raster vs vector). However, the ability of various sensors to measure specific geophysical parameters is not completely well understood; neither is the potential of combining images with proper data analysis into useful applications solutions. Another question is whether and how a combination of multi-sensor, multi-platform and multi-resolution data would create an added value to geoscientific work. There is a lack of proper tools to combine the data and to evaluate its usefulness. Therefore, when assessing the applicability of multi-source data synergy, problems of registration and the creation of multi-source data sets in a common ground reference system have to be solved in an optimal and user-friendly manner.

Since remote sensing data were first used in 1972, the requirements and standards for data rectification and integration has evolved due to different factors:

- the images have an off-nadir-viewing and the pixel size is smaller (10 m and less);

- the resulting products are digital;
- the interpretation of the products is done digitally (sometimes automatically) on a computer;
- the fusion of multisource data (sensor, platform) is common; and
- the integration of multiformat data (raster/vector) is increasing with geographic information system technology.

The registration of remote sensing data and their integration with vector data bases require then precise and robust geometric processing, as well as user friendly systems to meet these needs and standards. The polynomial, spline or kriging functions often used with images which have large distortions due to off-nadir viewing, fine resolution or airborne motion cannot achieve pixel accuracy or better. Furthermore, these methods correct distortions locally at the ground control points (GCPs), and do no take into account terrain elevation, which is a major factor in these distortions.

A large number of people still use these functions, not realizing the impacts on the data fusion and feature extraction. The resulting errors of this kind of geometric processing create mixels ("mixed pixels") in the radiometry of the composite image, thus generating wrong information or artefacts which do not correspond to the physical realities. Consequentely, the best available information from each image of the data set is not preserved in the composite ortho-images.

Considerable research has been carried out to develop robust and rigorous mathematical models describing the acquisition geometry related to different types of images (Visible and Infra-Red, VIR, and Synthetic Aperture Radar, SAR) and of platforms (spaceborne and airborne): for visible satellite images (Masson d'Autume, 1980; Sawada et al., 1981; Friedmann et al., 1983; Guichard, 1983; Toutin, 1983; Salamonowicz, 1986; Gugan, 1987; Konecny et al. 1987; Kratky, 1987; Paderes et al., 1989; Westin, 1990); for SAR satellite images (Rosenfield, 1968; Gracie et al., 1970; Leberl, 1978, Wong et al., 1981; Curlander, 1982; Naraghi et al., 1983; Guindon and Adair, 1992; Toutin and Carbonneau, 1992a); for visible airborne images (Gibson 1984; Ebner and Muller, 1986; Hofmann, and Muller, 1988); and for airborne SAR images (LaPrade, 1963, Rosenfield, 1968; Gracie et al., 1970; Derenyi, 1970; Leberl, 1972; Konecny and Schurr, 1984; Toutin et al., 1992) and many others.

Some studies reported promising results for one specific image or one specific platform. To date, no mathematical model and system can geometrically correct different images (visible and radar) from different platforms (spaceborne and airborne) precisely.

This paper will present a more general approach using an integrated and unified method and a user-friendly system to geometrically correct raw spaceborne and airborne, VIR and SAR images with a digital elevation model (DEM). The mathematical model is derived from the collinearity equations with photogrammetric method (Toutin, 1983). It integrates the complete viewing geometry with the position and the velocity of the

platform, with the parameters of the sensor and with the characteristics of the Earth and of the cartographic projection.

Quantitative and qualitative results will be presented for eight different types of images: MOS-MESSR, Landsat-TM, SPOT-XS/P, ERS-1 SAR, SEASAT-SAR, airborne SAR and airborne CCD MEIS sensor. The 1:50 000 digital topographic map is used to verify the accuracy.

2. INTEGRATED AND UNIFIED GEOMETRIC MODELLING

This geometric correction modelling was originally developed for SPOT-HRV (Guichard, 1983; Toutin, 1983) and tested on Landsat-TM (O'Brien and Handy, 1991), on MOS-MESSR and SEASAT-SAR (Toutin and Carbonneau, 1992a) and on airborne-SAR (Toutin et al., 1992). This approach has been now adapted in an operational environment at the Canada Centre for Remote Sensing (CCRS) as an integrated and unified geometric modelling, to geometrically process most of the commonly used remote sensing images.

The geometric modelling is integrated because in the final equations which represents the collinearity condition, it takes into account, the different distortions relative to the global geometry of viewing i.e.:

- the distortions relative to the platform (position, velocity, orientation);
- the distortions relative to the sensor (orientation angles, instantaneous field of view, detection signal integration time);
- the distortions relative to the Earth (geoid-ellipsoid including elevation); and
- the distortions relative to the cartographic projection (ellipsoid - cartographic plane).

The geometric modelling is unified because it has been adapted to indiscriminately process spaceborne or airborne data, and raw VIR and SAR data.

In summary, the collinearity equations of a ground point are first written in the instrumental reference system and converted into the cartographic projection system using elementary transformations (rotations and translations) which are functions of the parameters describing the distortions previously mentioned (Toutin, 1983). The model integrates the following transformations:

- rotation from the sensor reference to the platform reference;
- translation to the Earth's centre;
- rotation which takes into account the platform time variation;
- rotation to align the z-axis with the image centre (M_0) on the ellipsoid;
- translation to the image centre (M_0);
- rotation to align the y-axis in the meridian plane;
- rotation to have xM_0 y tangent to the ellipsoid;

- rotation to align the x-axis in the image scan direction; and
- rotation-translation into the cartographic projection.

The integration of the different distortions and the derivation of the equations are outside the scope of this paper, and are described for SPOT data by Toutin (1983), and for the SAR data in Toutin et al. (1992), and Toutin and Carbonneau (1992 a)

For example, with VIR data, the derivation of the equations has resulted in eight (8) unknowns for the modelling:

- the two cartographic coordinates of the image centre;
- the orientation at the image centre according to the cartograpbic North of the projection defined by the user;
- the two scale factors in along-track and across-track directions;
- the two parameter functions of the levelling angles in along-track and across-track directions; and
- a parameter function of the Earth rotation.

Each of these unknowns is in fact the combination of several correlated variables of the viewing geometry, so that the number of unknowns has been reduced to an independent set. As examples of combinations of several variables, we have:

- the orientation of the image is a combination of the platform heading due to orbital inclination, the yaw of the platform, the convergence of the meridian;
- the scale factor in along-track direction is a combination of the velocity, the altitude and the pitch of the platform, the detection signal time of the sensor, the component of the Earth rotation in the along-track direction; and
- the levelling angle in the across-track direction is a combination of platform roll, the viewing angle, the orientation of the sensor, the Earth curvature; etc.

For the SAR data, the images used are SAR standard products generally available to users. They are generated digitally during post processing from the raw signal SAR data (Doppler frequency, time delay). Errors present in the input parameters to the image geometry model will propagate through the image data. These include errors in the estimation of the slant range and of the Doppler frequency and also errors due to the satellite's ephemeris data and the ellipsoid. Assuming the presence of some geometric error residuals, the parameters of the geometric correction model reflect these residuals. Furthermore, the slant range direction distortions in radar are comparable to those encountered in oblique photographic viewing. The radar perspective represented in an image is portrayed as being orthogonal to the radar direction of illumination (Figure 1). Consequently, a viewing angle α of less than 90^0, usually employed on SAR systems, has about the same effect as an equivalent angle $90^0 - \alpha$ for the oblique optical viewing. Therefore, the elevation displacement occurs in the "opposite direction". Given this relationship, the applicability of the SPOT data, or any other optical model becomes more apparent. But, some known second order parameters of the geometric modelling for VIR

data are considered as unknowns for SAR data to take into account this relationship (Toutin et al., 1992).

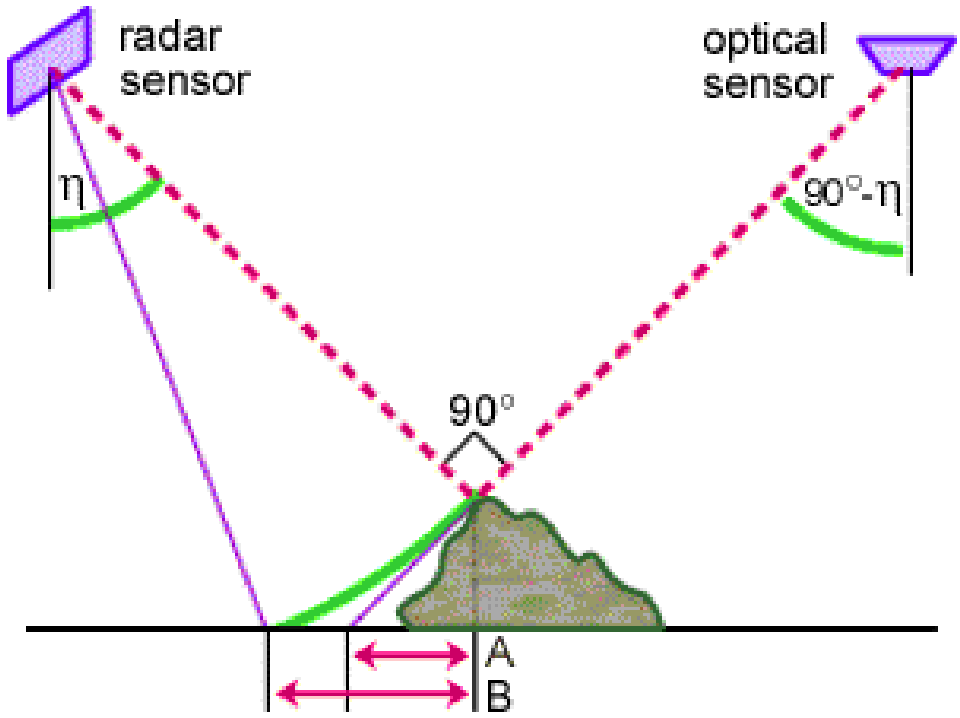

Figure 1: Relationship between the "radar image perspective" and the "visible image perspective". "A" is the elevation displacement away the optical sensor for the visble image, and "B" the elevation displacement towards the radar sensor for the radar image.

3. PROCESSING STEPS

Figure 2 is a flow chart of the geometric correction process used in this study.

The key processing steps are:

1. acquisition and pre-processing of the remote sensing data (images and if they exist, ephemeris and attitude);

2. acquisition and management of reference points (cartographic and image coordinates);

3. computation of the geometric correction model(s); and

4. ortho-image generation and mosaicking with a DEM.

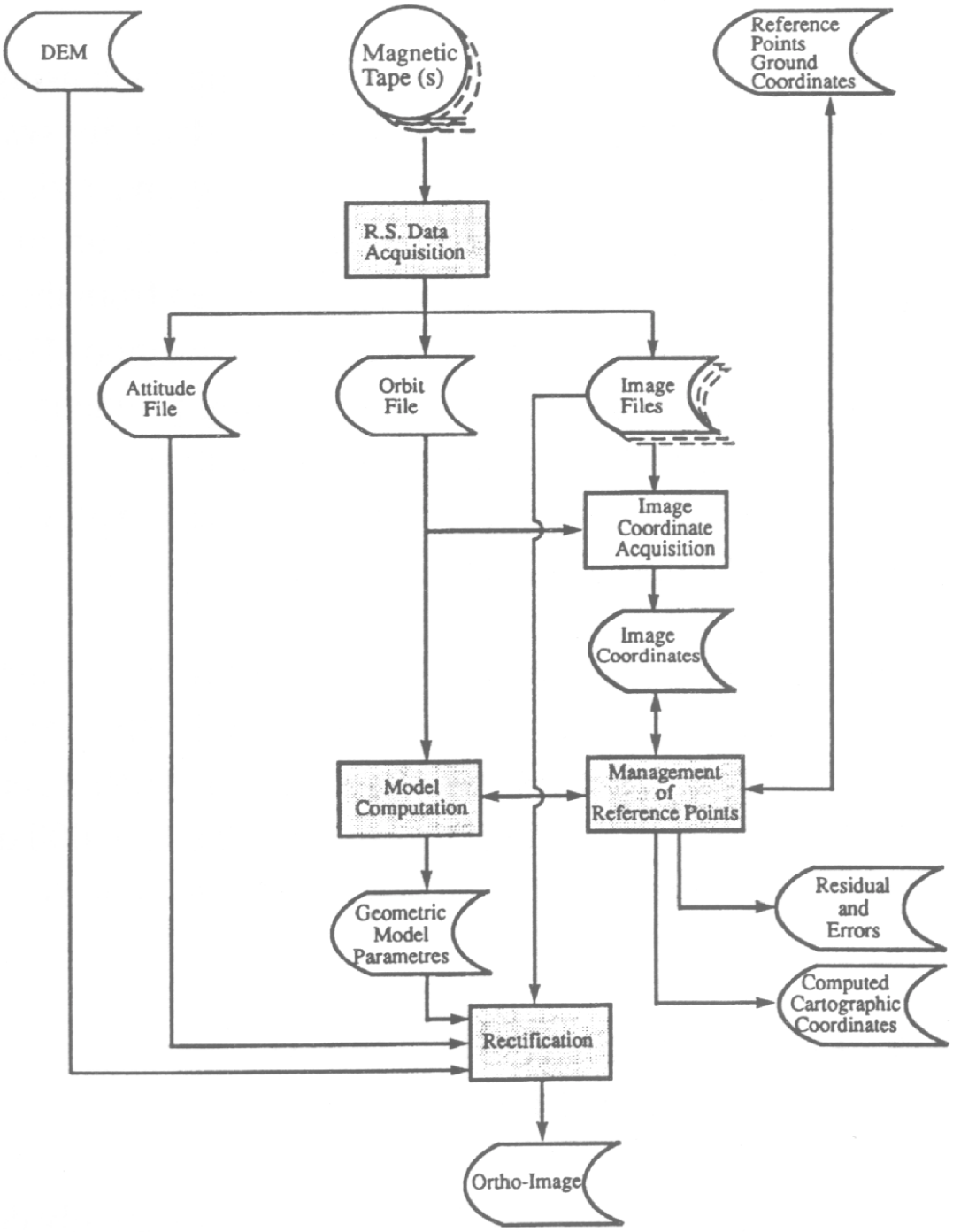

Figure 2: Flow chart of the geometric correction process. Tthe "shaded" rectangle are the four modules of the SRIT software.

In relation to these four steps, and to the geometric modelling, the software *SRIT "Système de Rectification des Images de Télédétection"* has been developed. This was originally done for satellite VIR data (Toutin et Carbonneau, 1992b), and later adapted to process airborne and satellite SAR data. It is now operational at CCRS and in Canadian private companies.

Here is a more detailed description of the different steps.The input data are:

- the images to be geometrically corrected, stored on magnetic tapes. They should be raw data for VIR and in slant or ground range presentation for SAR;
- the localization and the cartographic coordinates (XYZ) of the reference points;
- the DEM; the rectification process will address the DEM accuracy requirements.

The acquisition and the preprocessing of remote sensing data consists of reading the images and the ephemeris and attitude data, when available. The results are three types of files:

1. the attitude file gives the effect of the attitude variation on the ground for every line; this file only exists for VIR images;
2. the orbit file gives the geometry parameters. As an example for SPOT data, they are:

    - instantaneous field of view;
    - viewing angle;
    - detection signal integration time;
    - radial velocity;
    - angular speed;
    - earth centre - satellite distance;
    - satellite height;
    - orbital inclination;
    - ascending node longitude;
    - satellite argument on its orbit;
    - image centre coordinates (latitude, longitude, line, pixel);

3. the image files with one file for each spectral band. Radiometric preprocessing can be applied as linear stretched for VIR or speckle filtering for SAR.

There is no module for image visualization in the SRIT. Thus, the image coordinates can be acquired on any image analysis system. The definition of the reference points which are used in the geometric process is specific to each type of image because different sensors present different sensing geometries (incidence angle, resolution, etc.) and responses to illumination by the sun or the active sensing system; e.g. roads intersection are better defined on SPOT images, while river and lake intersections are more visible on ERS-1 SAR images. The accuracy of the geometric correction process depends mainly on the quality of the reference point in terms of image coordinates and cartographic

coordinates. The effort and the time spent on this processing step depends on the application and the accuracy the user wants to achieve.

The reference point management module enables the user to interactively visualize and manage the reference points, their coordinates (image and cartographic), their status (active or inactive), their types (control, homologous or tie, check), etc..

From this module, the geometric model can be computed. For each image to be processed, the orbital parameters are used first to initialize the geometric model: then an iterative least- square adjustment is used to solve the equation of observations with GCPs (each contributing to two equations). Four or seven GCPs are the minimum required to solve the 8 or 13 unknowns for VIR or SAR images, respectively. The adjustment procedure can be applied for one image and also simultaneously for images combining the equations of the different processed images. In this case, some tie points can be added to increase accuracy between the images. Each group of equations is then weighted as a function of the accuracy of the image data and of the cartographic data. Furthermore, complementary equations on some parameters have been added to take into account the accuracy of the ephemeris data, when available.

The results of these last two modules (point management and model computation) are:

- the geometric model parameters for each image;
- the residuals on the GCPs and the errors on the Independent Check Points, ICPs, (if any); and
- the computed cartographic coordinates for each point.

The last module is for the rectification to generate ortho-image and mosaics in the conformal cartographic projection system defined by the user (UTM, MTM, Lambert, etc). It uses the parameters of the geometric model determined in the least-square adjustment. Since the geometric model takes into account the elevation distortion, a DEM is needed to create more precise ortho-images. But if no DEM is available, different altitude levels can be input for different parts of the image to minimize this altimetric distortion. Figure 3 gives the planimetric error on the ortho-image as a function of the viewing angle and the DEM accuracy. These curves were mathematically computed with the elevation distortion parameters of the geometric modelling. For example, for a SPOT image acquired with a viewing angle of 10^0 and with a 45-m DEM accuracy, the error generated on the ortho-image is 9-m. Inversely, if a 4-m planimetric accuracy for the ortho-image is required with a 10-m DEM accuracy, the image should be acquired with a viewing angle less than 20^0. The same curves can be applied to SAR data by using the right angle complement of the viewing angle as shown in Figure 1.

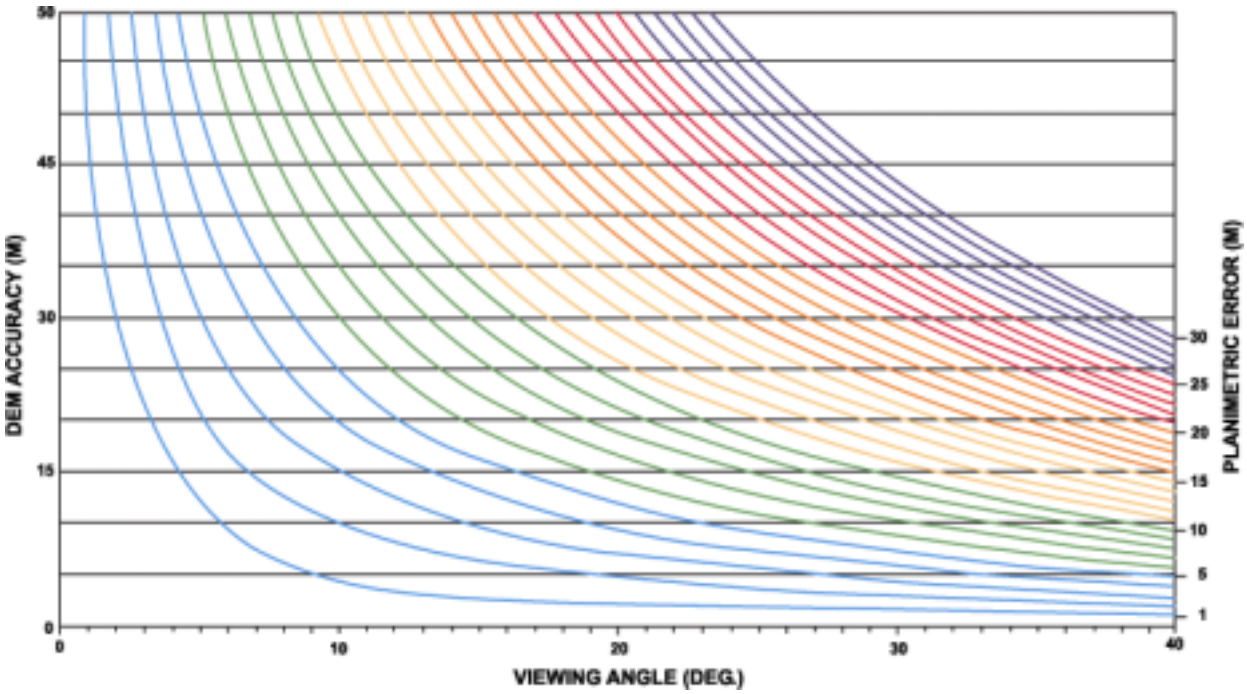

Figure 3: Relationship between the acquisitionviewing angle, the DEM accuracy and the planimetric error on the ortho-image.

In summary, the main user- friendly characteristics of this method and system are:

- it is the same to operate for any image;
- throughout the processing steps, the user does not have to worry about the type of images. The relevant information on the images(s) is taken directly from the tape, and transferred to the other processing steps;
- the user can process and tie one, two or more images together in the least square adjustment, giving a better relative accuracy between the different ortho-images and mosaics;
- other satellite and airborne data (IRS, JERS-1,Radarsat, MOMS,) can be added easily ; and
- the user controls the full process from the input of raw images to the production of ortho-images. Error propagation can be monitored and the data (GCP and DEM accuracies, image viewing angle, ...) can be selected accordingly to fit the accuracy requirements of the application (Figure 3).

4. DATA SET

The topographic data are the Sherbrooke Data Set for the topographic applications of remote sensing (Lassere et Lemieux, 1990). The study area is made up of two half map sheets of the province of Quebec (Canada), and represents land coverage of

approximately 26 x 40 km, with an altitude variation of about 350 metres. The data used in this experiment are:

- 235 reference points which have been obtained using an STK-1 stereocomparator. The root mean square error of the cartographic coordinates are better than three metres. These points are mainly intersections of expressways, highways, roads, streets or railroads. Of these 235 points, 215 are located in the two half map sheets, and the other 20 are outside. This distinction between the reference points is useful in subsequent tests of the geometric modelling;

- a DEM with a 50-m grid, generated from the 1:50 000 contour lines (10-m intervals). The accuracy is in the order of five metres;

- the vector data of the digital topographic map. All the elements are positional data, as observed on the surface of the Earth in X, Y and Z coordinates and without movement of the element due to cartographic generalization. The accuracy is in the order of five meters.

The remote sensing data are summarized in Table 1. There are eight types:

- six acquired by spaceborne platforms (MOS, Landsat, SPOT, SEASAT, ERS) and two by airborne platforms (Falcon, Convair) ; or, according to sensor
- five VIR (MESSR, TM, XS, P, MEIS) and three SAR.

The VIR data have been linearly stretched over 8 bits. No radiometric processing has been applied to the SAR data.

5. RESULTS

5.1 Quantitative Results

The number of points (of the 235 reference points) acquired on each image and their accuracy vary according to the spectral response of each sensor, which can affect feature visibility and the shape and appearance of the targets. The image coordinate accuracies are 1/3 to 1/2 of pixel for VIR data and one to two pixels for SAR data.

Two tests have been performed for the quantitative results analysis:

- Test 1: all the identifiable reference points have been used as GCPs for each image to compute the geometric model (e.g. for SPOT-P 139 GCPs and for ERS-1 SAR 25 GCPs). Therefore, there are no ICP; and
- Test 2: only the identifiable reference points (of the 20)outside the map sheets have been used as GCPs for each image to compute the geometic model (e.g. for SPOT-P, 19 GCPs, and for ERS-1 SAR, 10 GCPs). The other reference points (of the 215) inside the map sheets are used as ICPs to check the accuracy (e.g. for SPOT-P, 120 ICPs, and for ERS-1 SAR 15 ICPs).

Table 2 gives the full results of two modelling tests with the root mean square (RMS) and maximum residuals on the GCPs, and the RMS, maximum and bias errors on the ICPs. The residuals reflect the modelling accuracy, and the errors reflect the restitution accuracy. As the plotting error on the ICPs is included, the ortho-image accuracy is better than the restitution accuracy.

In contrast to polynomial methods, which are sensitive to the number and spatial distribution of the GCPs and their elevation, this model is not affected by these factors because it retains the complete geometry of viewing precisely, including the terrain given that there is no extrapolation in planimetry and also in altimetry. These issues have been already addressed quantitatively for different data in previous research (Toutin and Carbonneau, 1989, 1992a). The same research has shown that eight GCPs is a good compromise to get the same accuracy, as shown in Table 2, because the geometric modelling corrects the image globally, when the polynomial modelling corrects locally.

In the first test, as the RMS residuals are on the same order of magnitude as the plotting error (1/3 - 1/2 pixel for satellite VIR images and 1 - 2 pixels for the others) and as the maximum error is less than three times the RMS residuals (this statement is also valid for the second test on the GCPs and ICPs), the mathematical model properly describes the viewing geometry of image acquisition, but it is also stable and robust for the full image without generating local errors. Furthermore, as the bias errors on the ICP for the second tests are small, the mathematical model does not introduce trends or systematic errors. These results give a good level of confidence for the geometric correction and rectification of all these types of images with different terrain and geometric configurations.

In summary, the general results are:

- one third of pixel accuracy for the satellite VIR data; and
- one to two pixel accuracy for the other data (SAR and airborne)

For the MOS-MESSR image, the results are half pixel because no ephemeris and attitude data were available; and in optical systems, angles are one of the important keys. When attitude data are available, the same one-third of pixel accuracy could be achieved.

For the SAR satellite images, the pixel spacing is 12.5 metres, but the resolution cell is 25-30 metres. To maintain consistency for comparison with VIR image accuracies, this results in one-half to one pixel resolution cell accuracy for satellite SAR images and one to two resolution cells for airborne images. Furthermore, no ephemeris data was available for the SAR images.

For the airborne images, the difference in results may be explained by the airborne motion which is less stable than the satellite. High frequency distortion cannot be corrected without precise attitude and position data.

Platform	Sensor	Level of Processing	Acquisition Date	Supplemental Data	Ground Coverage (km)	Pixel Size (m)	Viewing Angles (deg)
Convair	SAR-C-HH	slant range	90/09/11	yes	16 x 40	4 x 4.31	45 / 76
Falcon	CCD-MEIS	raw	90/06/11	yes	6 x 40	5 x 4	-20 / +20
SPOT	HRV-P	raw	87/06/20	yes	70 x 60	12 x 10	27.2/31.3
ERS-1	SAR-C-VV	ground range	92/06/16	no	100 x 100	12.5 x 12.5	21 / 25
SEASAT	SAR-L-HH	ground range	78/09/17	no	100 x 100	12.5 x 12.5	19 / 25
SPOT	HRV-XS	raw	87/08/02	yes	60 x 60	22 x 20	-10.7 / -6.6
LANDSAT	TM	bulk	89/08/27	yes	88 x 94	30 x 30	0 / 7
MOS	MESSR	raw	89/06/22	no	100 x 100	50 x 50	-3 / +3

TABLE 1: CHARACTERISTIC OF THE IMAGE DATA SET

TABLE 2: RESULTS OF THE GEOMETRIC CORRECTION FOR THE TWO TESTS

Test	Image		MESSR		TM		HRV-XS		SEASAT-SAR		ERS1-SAR		HRV-P		MEIS		SAR	
1	GCP Number / ICP Number		89 / 0		95 / 0		154 / 0		24 / 0		25 / 0		139 / 0		69 / 0		44 / 0	
	Res.		X	Y	X	Y	X	Y	X	Y	X	Y	X	Y	X	Y	X	Y
	GCP	RMS	18.3	17.2	13.1	9.5	7.1	7.0	13.7	11.7	22.3	21.1	3.4	3.1	6.1	5.3	6.6.	5.6
		MAX	-45.1	37.3	-32.8	26.7	-20.9	-18.8	-30.8	-22.4	-42.5	-50.8	-8.7	-9.0	15.4	-12.4	13.1	-16.9
2	GCP Number / ICP Number		12 / 77		17 / 72		19 / 135		10 / 14		10 / 15		19 / 120		12 / 57		12 / 32	
	Res / Error		X	Y	X	Y	X	Y	X	Y	X	Y	X	Y	X	Y	X	Y
	GCP	RMS	16.2	13.2	10.7	6.6	6.3	7.0	15.1	7.8	12.2	25.0	2.7	3.1	4.7	9.0	6.3	4.9
		MAX	-38.4	25.2	-17.6	-16.0	12.1	16.3	-30.8	-14.2	23.1	32.3	-5.0	7.6	-8.3	-17.5	-10.2	-9.9
	ICP	**RMS**	**23.4**	**20.5**	**12.5**	**10.1**	**8.0**	**8.2**	**18.8**	**14.7**	**39.9**	**20.1**	**3.8**	**3.4**	**7.3**	**7.5**	**10.9**	**6.0**
		MAX	-55.8	45.9	23.8	22.9	23.7	-23.6	35.5	-29.3	-75.8	32.3	-8.7	-9.9	-15.0	-18.1	-24.4	-20.2
		BIAI	-9.2	-3.9	-1.9	4.6	3.5	-4.5	7.5	-1.4	-1.7	5.3	1.4	-0.1	0.4	0.0	0.3	-0.3

5.2 Qualitative Results

Finally, with the last SRIT module, ortho-images have been generated for the different images, using a DEM. That enables more complex products such as mosaics or colour composite images to be created.

Figure 4 is a mosaic of the eight ortho-images previously described. The image is 39 x 29 km large with a common 10-m pixel size. From west to east, or north to south, there are the airborne SAR (C-HH), airborne CCD-MEIS sensor, SPOT-P, ERS-1-SAR (C-VV), SEASAT-SAR (L-HH), SPOT-XS (Band 2) , Landsat-TM (Band 3)and MOS-MESSR (Band 2). The mosaic becomes fuzzy when viewed diagonally from the 4-m (airborne data) to the 50-m (MOS-MESSR) pixel size, resampled at 10 metres.

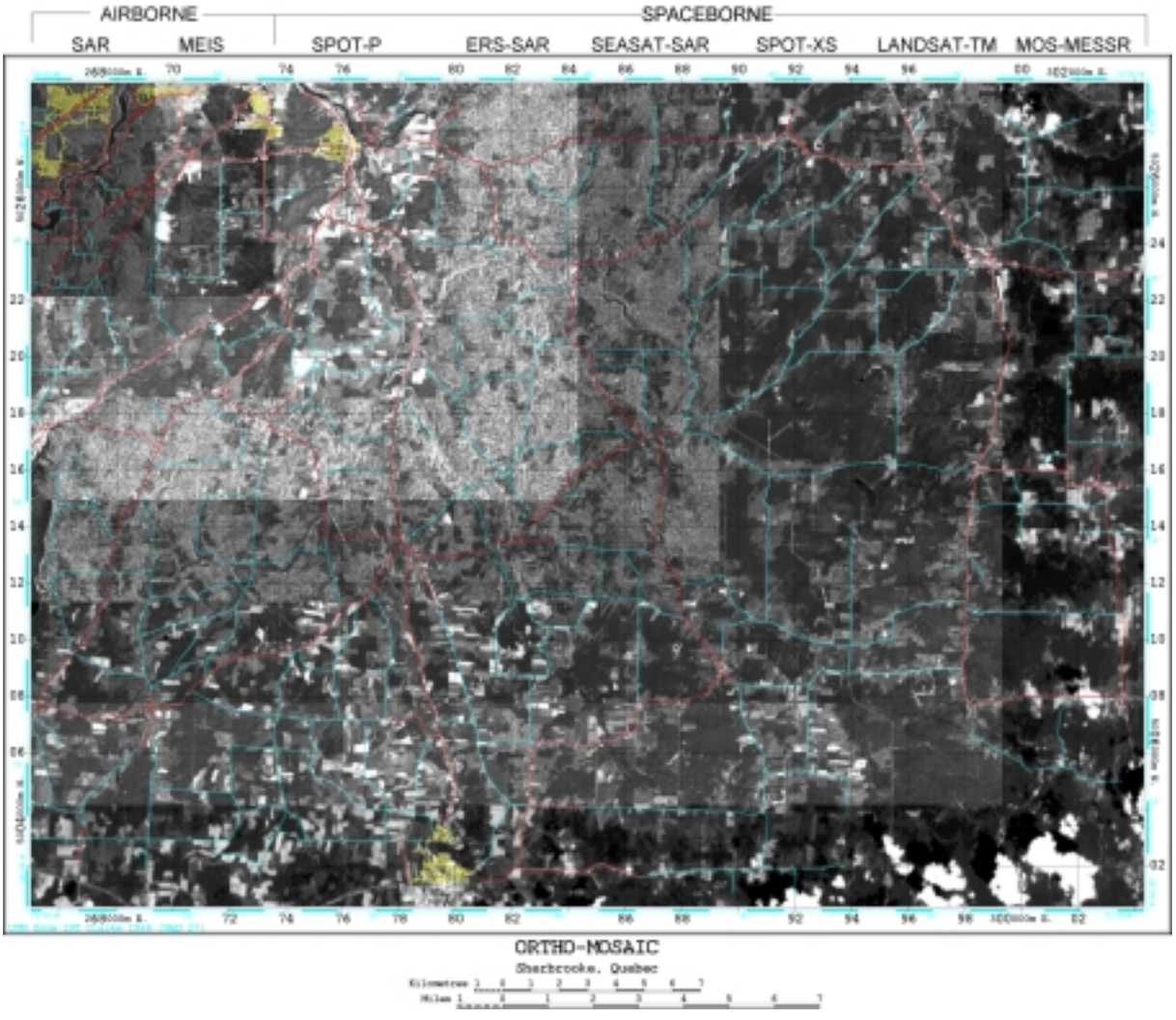

Figure 4: Ortho-mosaic of the two aiborne and six satelliteVIR and SAR images (39 km by 29 km; 10-m pixel spacing) with the road network (red: main; blue: secondary; yellow: city).

This Figure displays a mean pixel intensity difference for the different sensors; it is particularly evident for ERS-1. These differences are mainly due to the following factors:

- the image sensor wave-lengths are quite different;
- the dynamic range is specific to each sensor (HRV, MESSR, TM, SAR, etc.) and to each spectral band (visible, L, C). Furthermore, linear stretch (on 8 bits) for VIR increases the variation in the dynamic range;
- for the SAR, the system configurations are completely different: the sensor response is related to the frequency, to the polarization (VV penetrates vegetation less than HH), and also to the incidence angle. Furthermore, the dielectric constant is related to the frequency; and
- the data has not been absolutely calibrated.

However in this study, the calibration was not an important issue because the purpose of the research was not to extract and compare radiometric responses related to geophysical parameters. Figure 5 is an enlargement (17 x 15 km) in the North-West part of the Figure 4 with the road network overlaid.

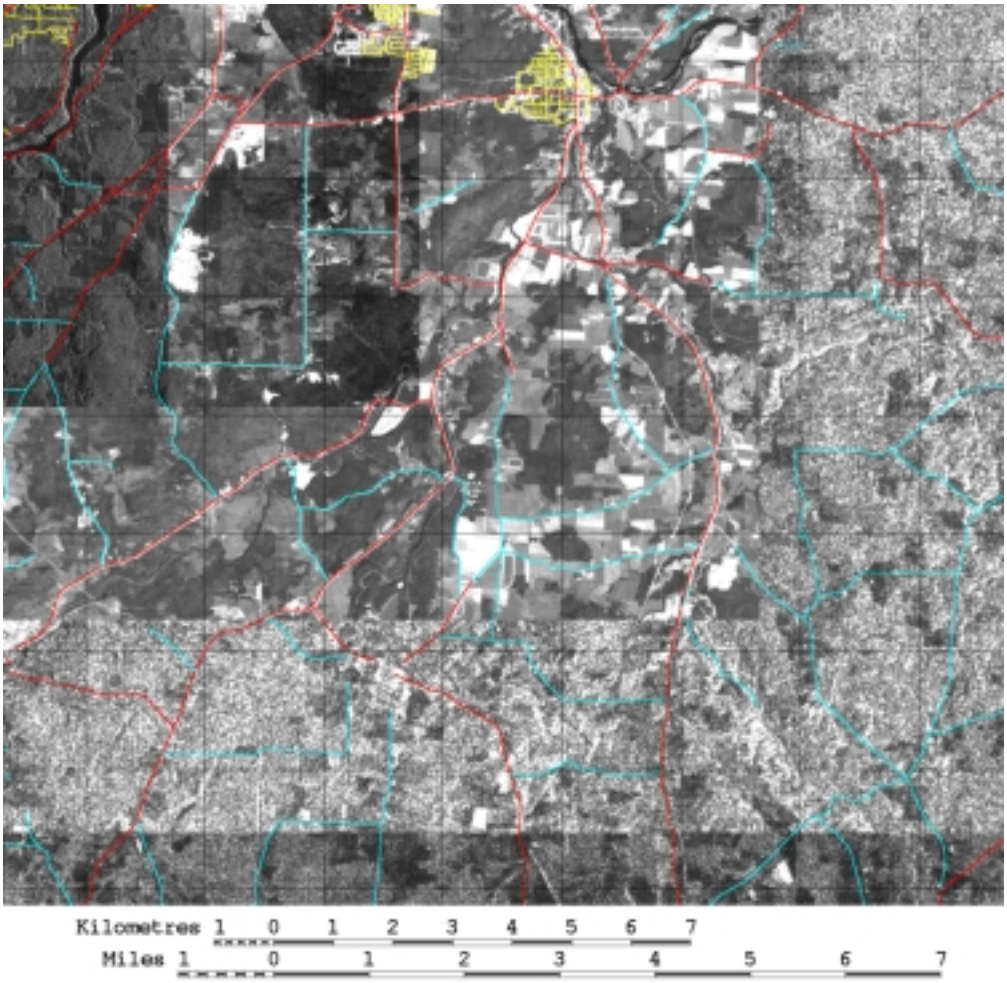

Figure 5: Enlargement of the NW part of the previous ortho-mosaic with the road network.

Figure 6 is also an enlargement (10 x 10 km) in the North-West of a colour composite ortho-image of SPOT-P and two airborne SAR from opposite-side flight lines using the intensity-hue-saturation coding (SAR to intensity and saturation and SPOT-P to hue). The roads network has been overlaid. The pixel size of this image is five metres, which is a good compromise between the original 4-m and 10-m pixel sizes of airborne SAR and SPOT-P images, respectively.

Figure 6: Enlargement of a colour composite ortho-image of SPOT-PLA and two airborne SAR (10 km by 10 km; 5-m pixel spacing)

The qualitative viewing of these ortho-mosaics and colour composite ortho-image confirms the quantitative results of 1/3 to 1/2 pixel accuracy for VIR satellite images and one to two pixel accuracy for the other images. Linear features are good elements to verify visually the quality of

the mosaicking. Some roads and power line clearcuts have been marked on Figure 4 with the letters “a” and “b” respectively; there is no discontinuity in both X and Y directions at the junction between the different images. In some areas, maximum errors appear (20 m for airborne CCD sensor and SAR; 50-60 m for spaceborne SAR) in accordance with the statistics of Table 2. There is no strong local distortion, greater than the tolerance; that is one of the qualities of this geometric modelling which corrects the images globally. The topographic file has an accuracy of five meters, which is in the same order of magnitude as errors on some images (SPOT and airborne). Therefore, the topographic file cannot be considered as an absolute reference, when compared to SPOT data or airborne data.

Futhermore, Figure 6 shows qualitatively that this geometric correction method adapted to the nature and the characteristics of the images generates high quality colour composite images, which are sharp and precise containing well defined cartographic elements and information that are easy to interpret.

6. CONCLUSIONS

This paper has shown a method and a system with a DEM to geometrically correct raw images. The mathematical model is based on the collinearity condition and represents the physical realities of the full viewing geometry, platform- sensor-Earth. The method has been tested at CCRS on different images (SPOT-HVR, Landsat-TM, MOS-MESSR, SEASAT-SAR, ERS-1 SAR, airborne VIR and SAR). The method and the mathematical model are now integrated and unified to process indiscriminately images from different sensors (VIR and SAR) on different platforms (spaceborne and airborne) from different resolutions.

The operational SRIT software, based on this method with DEM, enables the generation of ortho-images and mosaics of the previously mentioned images. Because the information relative to the platform and the sensor are directly extracted from the tape and transferred to the other processing steps the user does not have to consider image type, except for the GCP acquisition step. One of the major advantages of the method is that only one image correction system is needed for different types of sensors and platforms. Since this initial research, the system has been now adapted and tested for processing other data sources: the airborne SAR images from the Jet Propulsion Laboratory (USA), the SAR images from the shuttle SIR-C, the images from JERS-1 and the LISS images from the Indian Remote Sensing satellite. In the near future, it will be adapted for other data (MOMS, RADARSAT).

Processing different images MOS-MESSR, Landsat-TM, SPOT-P/XS, SEASAT-SAR, ERS-1 SAR, airborne SAR and CCD sensors, this method has achieved accuracies of:

- 1/3 of pixel for satellite VIR images;
- 1 resolution cell for satellite SAR images; and
- 1-2 resolution cells for airborne images.

The difference in the result are due to:

- a better definition and quality of the GCPs on VIR images; and
- a better stability and knowledge of the spaceborne path than the airborne path.

Using a DEM, different ortho-images and their fusion (mosaics, colour composite) have been generated to qualitatively check the relative accuracy between the different ortho-images. Linear features are used to visually verify the connection between the images. The road network has been overlaid to check the absolute accuracy. It confirms the quantitative results on check points, but for some data (SPOT and airborne), the road network cannot be used as an absolute reference, because it has an accuracy of five metres, the same order of magnitude as the SPOT ortho-image accuracies (3 m for P; 7 m for XS) and as the airborne ortho-image accuracies (7.5 m for CCD-MEIS; 6 - 10 m for SAR).

7. ACKNOWLEDGEMENTS

The author would like to thank the Canada Centre for Geomatics for providing the digital topographic data and for their participation in the SRIT development. He also thanks Mr. Yves Carbonneau and Ms. Liyuan Wu of Consultants TGIS Inc. for their collaboration in the SRIT development and for the data processing.

8. REFERENCES

1. Curlander, J.C., 1982, Location of Spaceborne SAR Imagery, IEEE Transaction of Geoscience and Remote Sensing, GE-22 (2), pp: 106-112

2. Derenyi, E.E., 1970, An Exploratory Investigation into the Relative Orientation of Continuous Strip Imagery, Research Report No. 8, University of New Brunswick, Canada.

3. Ebner H., and Muller F., 1986, Processing of Digital Three Line Imagery Using a Generalized Model for Combined Point Determination, International Archives of Photogrametry and Remote Sensing, 26(311), pp. 212-222.

4. Friedmann, D.E., Friedel, J.P., Magnussen, K.L., Kwok, and R. Richardson, 1983, Multiple Scene Precision Rectification of Space-borne Imagery with very few Control Points, Photogrammetric Engineering and Remote Sensing, 49(12), pp 1657-1667.

5. Gibson, J., 1984, Processing Stereo Imagery from Line Imagers, 9th Canadian Symposium on Remote Sensing, (Canada) pp. 471-488.

6. Gracie, G., Bricker, J.W., Brewer, R.K., and Johnson, R.A., 1970, Stereo Radar Analysis, U.S. Engineer Topographic Laboratory, Report No. FTR-1339-1, Ft. Belvoir, VA, U.S.A.

7. Gugan, D.J., 1987, Practical Aspects of Topographic Mapping from SPOT Imagery, Photogrammetric Record, 12 (69), pp 349-355.

8. Guichard, H., 1983, Etude théorique de la précision dans l'exploitation cartographique d'un satellite à défilement : application à SPOT, Société Française de Photogrammétrie et de Télédétection, 90(2), pp. 15-26.

9. Guindon B., and Adair, M., 1992, Analytic Formulation of Spaceborne SAR Image Geocoding and Value-Added Products Generation Procedures Using Digital Elevation Data, Canadian Journal of Remote Sensing, 18 (1), pp. 2-12.

10. Hoffmann, O., and Muller, F., 1988, Combined Point Determination Using Digital Data of three line Scanner Systems. International Archives of Photogrammetry and Remote Sensing, 27 (B11) pp. III / 567 - III / 577.

11. Konecny, G., and Schuhr, W., 1984, Practical Results of Geometric SAR-580, Image Evaluation, International Archives for Photogrammetry and Remote Sensing, 25 (A3).

12. Konecny, G., Lohmann, P., Engel, H., and Kruck, E., 1987, Evaluation of SPOT Imagery on Analytical Instruments, Photogrammetric Engineering and Remote Sensing, 53(a), p.p. 1223-1230.

13. Kratky, V., 1987, Rigorous Stereophotogrammetric Treatment of SPOT Images. Compte rendus du Colloque International sur SPOT-1 : utilisation des images, bilans, résultats, Paris, France, pp. 1281-1288.

14. La Prade, G.L., 1963, An Analytical and Experimental Study of Stereo for Radar, Photogrammetric Engineering, 29(2), pp. 294-300.

15. Lassere, M., and Lemieux, J.P., 1990, Sherbrooke Data Set for Topographic Applications of Remote Sensing. Final Report, EMR Canada, 40 pages.

16. Leberl, F., 1972, On Model Formation with Remote Sensing Imager, Oesterr, Zeitschrift fur Vermessungswesen und Photogrammetrie, 60(2), pp. 43-61.

17. Leberl, F., 1978, Satellite radargrammetric, Deutsche Geodactische Kommission, Munich, Germany, Serie C, 239, 156 pages.

18. Masson d'Autume, M. G., 1980, Le traitement géométrique des images de télédétection, Annales des Mines, Paris, France, 2, pp. 53-62.

19. Naraghi, M., Stromberg, W., and Daily, M., 1983, Geometric Rectification of Radar Imagery using Digital Elevation Models, Photogrammetric Engineering and Remote Sensing, 49(2), pp. 195-159.

20. O'Brien, D., and Handy, J., 1991, Recent Image Mapping Experiments in the Surveys, Mapping and Remote Sensing Sector, National Conference on GIS, Ottawa, Ontario, Canada, pp. 458-470.

21. Paderes, F.C.., Mikhail, E.M., Fagerman, J.A., 1989, Batch and On-line Evaluation of Stereo SPOT Imagery. Proceedings of the ASPRS - ACSM Convention, Baltimore, MD, U.S.A., Vol. 3, pp. 31-40.

22. Rosenfield, G.H., 1968, Stereo Radar Techniques, Photogrammetric Engineering, 34(6), pp. 586-594.

23. Salamonowicz, P.H., 1986, Satellite Orientation and Position for Geometric Correction of Scanner Imagery. Photogrammetric Engineering and Remote Sensing, 52(4), pp. 491-499.

24. Sawada, N., Kikode, M. Shinoda, H, Asada, H., Iwanaga, M., Watanabe, S., and Mori, K., 1981, An Analytic Correction Method for Satellite MSS Geometric Distortion, Photogrammetric Engineering and Remote Sensing, 47 (8), pp. 1195-1203.

25. Toutin, Th., 1983, Analyse mathématique des possibilités cartographiques du satellite SPOT, Mémoire de DEA, Ecole Nationale des Sciences Géographiques, France, 74 pages.

26. Toutin Th., et Carbonneau, Y., 1989, La multi stéréoscopie pour les corrections d'images SPOT-HRV, Journal Canadien de télédétection, 15(2), pp. 110-119.

27. Toutin, Th., and Carbonneau, Y., 1992 (a), MOS and SEASAT Image Geometric Corrections, IEEE Transactions on Geoscience and Remote Sensing, 30(3), pp. 603-609.

28. Toutin, Th., and Carbonneau, Y., 1992b, La création d'ortho-images : description d'un nouveau système, Journal canadien de télédétection, 18(3), pp. 136-141.

29. Toutin, Th., Carbonneau, Y., and St. Laurent L., 1992, An Integrated Method to Rectify Airborne Radar Imagery using DEM, Photogrammetic Engineering and Remote Sensing,(58(4), pp. 417-422.

30. Westin, T., 1990, Precision Rectification of SPOT Imagery, Photogrammetric Engineering and Remote Sensing, 56(2), pp. 247-253.

31. Wong, F., Orth, R., and Friedmann, D., 1981, The Use of Digital Terrain Model in the Rectification of Satellite-Borne Imagery, 15th International Symposium on Remote Sensing of Environment, Ann Arbor, Michigan, U.S.A., pp. 653-662.